REPORT DOCUMENTATION PAGE

Form Approved
OMB No. 0704-0188

1. REPORT DATE *(DD-MM-YYYY)*
17-05-2004

REPRINT

4. TITLE AND SUBTITLE
Probing the Magnetic Polarity Structure of the Heliospheric Current Sheet

5a. CONTRACT NUMBER

5b. GRANT NUMBER

5c. PROGRAM ELEMENT NUMBER
61102F

6. AUTHOR(S)
S.W. Kahler, N.U. Crooker*, and D.E. Larson**

5d. PROJECT NUMBER
2311

5e. TASK NUMBER
RD

5f. WORK UNIT NUMBER
A1

7. PERFORMING ORGANIZATION NAME(S) AND ADDRESS(ES)
Air Force Research Laboratory/VSBXS
29 Randolph Road
Hanscom AFB MA 01731-3010

9. SPONSORING / MONITORING AGENCY NAME(S) AND ADDRESS(ES)

10. SPONSOR/MONITOR'S ACRONYM(S)
AFRL/VSBXS

11. SPONSOR/MONITOR'S REPORT NUMBER(S)
AFRL-VS-HA-TR-2004-1088

12. DISTRIBUTION / AVAILABILITY STATEMENT
Approved for Public Release; Distribution Unlimited.

*Center for Space Res, Boston University, MA; **Space Sciences Lab, Univ of California, Berkeley, CA

13. SUPPLEMENTARY NOTES
REPRINTED FROM: JOURNAL OF GEOPHYSICAL RESEARCH, Vol 108, No. A8, 1316, doi: 10.1029/2002JA009649, 2003.

14. ABSTRACT
We use solar wind heat-flux electrons to determine the solar magnetic polarities of the inter-Planetary magnetic field (IMF) close to the heliospheric current sheet (HCS) around the time of the last solar minimum in 1995-1996. At that time the tilt angle of the HCS was very low and solar activity was minimal, allowing the Wind spacecraft to probe the polarities of the fields close to the HCS during a time relatively free of transient interplanetary coronal mass ejections (ICMEs). During the three periods we examined, all solar polarity boundaries predicted from Stanford source surface (SS) maps were observed. During 34 days in which the SS magnetic neutral line skimmed within 3 deg of the ecliptic, only six tangential excursions into opposite solar polarities were observed. The distribution of the durations of magnetic polarity sectors was very similar to that reported earlier for solar maximum in 1978-1982, showing no increase in sectors which might be expected for a spacecraft trajectory roughly tangential to a corrugated HCS separating regions of opposite polarity.

15. SUBJECT TERMS
Interplanetary magnetic fields
Heat-flux electrons
Heliospheric current sheet
Magnetic sector boundaries

16. SECURITY CLASSIFICATION OF:			17. LIMITATION OF ABSTRACT	18. NUMBER OF PAGES	19a. NAME OF RESPONSIBLE PERSON
a. REPORT		c. THIS PAGE			S. W. Kahler
UNCLAS	UNCLAS	UNCLAS	SAR	9	19b. TELEPHONE NUMBER *(include area code)* 781-377-9665

JOURNAL OF GEOPHYSICAL RESEARCH, VOL. 108, NO. A8, 1316, doi:10.1029/2002JA009649, 2003

Probing the magnetic polarity structure of the heliospheric current sheet

S. W. Kahler
Space Vehicles Directorate, Air Force Research Laboratory, Hanscom Air Force Base, Massachusetts, USA

N. U. Crooker
Center for Space Physics, Boston University, Boston, Massachusetts, USA

D. E. Larson
Space Sciences Laboratory, University of California, Berkeley, California, USA

Received 16 August 2002; revised 4 March 2003; accepted 4 April 2003; published 13 August 2003.

[1] We use solar wind heat-flux electrons to determine the solar magnetic polarities of the interplanetary magnetic field (IMF) close to the heliospheric current sheet (HCS) around the time of the last solar minimum in 1995–1996. At that time the tilt angle of the HCS was very low and solar activity was minimal, allowing the Wind spacecraft to probe the polarities of the fields close to the HCS during a time relatively free of transient interplanetary coronal mass ejections (ICMEs). During the three periods we examined, all solar polarity boundaries predicted from Stanford source surface (SS) maps were observed. During 34 days in which the SS magnetic neutral line skimmed within 3° of the ecliptic, only six tangential excursions into opposite solar polarities were observed. The distribution of the durations of magnetic polarity sectors was very similar to that reported earlier for solar maximum in 1978–1982, showing no increase in sectors which might be expected for a spacecraft trajectory roughly tangential to a corrugated HCS separating regions of opposite polarity. The heat-flux electron pitch angle distributions, intervals of magnetic false polarities, high-latitude field excursions, and orientations of minimum variance vectors at polarity boundaries were all similar to those observed away from the boundaries. About one third of the polarity boundaries were displaced from the large-angle changes of the IMF direction usually thought to define the HCS. These observations suggest a single, globally smooth HCS in the form of a corrugated ribbon much less complex than and often separated from a thicker and more structured surrounding current sheet system formed by IMF discontinuities. *INDEX TERMS:* 2134 Interplanetary Physics: Interplanetary magnetic fields; 2169 Interplanetary Physics: Sources of the solar wind; 7524 Solar Physics, Astrophysics, and Astronomy: Magnetic fields; *KEYWORDS:* heliospheric current sheet, heat-flux electrons, source surface maps, magnetic sector boundaries

Citation: Kahler, S. W., N. U. Crooker, and D. E. Larson, Probing the magnetic polarity structure of the heliospheric current sheet, *J. Geophys. Res.*, *108*(A8), 1316, doi:10.1029/2002JA009649, 2003.

1. Introduction

1.1. Heliospheric Current Sheet Structure

[2] The heliospheric current sheet (HCS) is defined as the boundary between outward directed and inward directed open heliospheric magnetic fields. These fields are the extension of the solar magnetic field, which to first order is a dipole tilted with respect to the solar rotational axis. The outward convection of the fields by the solar wind from the rotating Sun causes the HCS to form a series of peaks and valleys that spiral outward [*Thomas and Smith*, 1981]. The long-lived (approximately days) regions of fields of a single dominant magnetic polarity observed at 1 AU between passages of the HCS constitute the magnetic sector structure. The deduced solar source regions of the HCS generally match well the calculated location of the magnetic neutral line on a solar source surface at which the magnetic field is assumed radial [*Behannon et al.*, 1989; *Arge and Pizzo*, 2000; *Smith*, 2001].

[3] Some properties of the HCS structure, such as the tilt and global shape of the sheet, are known with confidence. Early observations used the interplanetary magnetic field (IMF) directions observed on the Helios 1 and Helios 2 spacecraft between 0.3 and 1 AU to deduce that the HCS near the Sun was not flat but warped [*Villante et al.*, 1979]. The planes of rotation of the vector fields at the sector boundaries (SBs), assumed to be the HCS, were determined from minimum variance analysis to be highly inclined ($\geq$45°) to the ecliptic plane [*Klein and Burlaga*, 1980; *Behannon et al.*,

0148-0227/03/2002JA009649$09.00

1981; *Villante and Bruno*, 1982]. *Behannon et al.* [1981] suggested a model in which the high inclinations are due to corrugations of scale length 0.05 to 1 AU on a HCS with a low inclination on a global scale.

[4] The structure transverse to the surface of the HCS, on the other hand, has been poorly understood. Sector boundary (SB) crossings of IMP 6 were sometimes found to be sharp (<10 min), but a class of complex, or thick (≥3 hours), crossings was also found [*Klein and Burlaga*, 1980]. The existence of the thick SBs with multiple current sheet crossings was confirmed by *Behannon et al.* [1981] with 142 field directional discontinuities in a set of 25 SBs observed on Helios 1. Similarly, an analysis of 20 SBs observed in 1994–1995 with the magnetometer experiment on the Wind spacecraft found a total of 212 large-angle field discontinuities [*Lepping et al.*, 1996].

1.2. Heat-Flux Electron Probes of Magnetic Polarity

[5] The inferred complexity of the HCS is based on the assumption that the solar magnetic polarities of the IMF are correctly deduced from a comparison of the observed IMF directions with the Parker spiral field direction. A technique to test that assumption uses the fact that solar energetic electrons will stream antisunward along field lines, even if the fields are locally turned backward toward the Sun [*Kahler and Lin*, 1994; *Kahler*, 1997]. *Kahler and Lin* [1995] used that technique with 2 keV electrons observed on the ISEE-3 spacecraft to examine apparent SBs in 1978–1979. Contrary to the basic assumption, they found that the field rotation angle $\omega \leq 90°$ for about half the magnetic polarity changes and that about half of the $\omega > 120°$ field rotations were not polarity changes.

[6] The technique to deduce solar magnetic polarities was adapted to the lower-energy ($E < 1$ keV) solar wind heat-flux electrons observed on ISEE-3 to study periods within well defined magnetic sectors when the field directions appeared to be reversed from the normal spiral direction of the sector. About half those periods, called intrasector field reversals (IFRs), were associated with bidirectional electron (BDE) flows [*Kahler et al.*, 1996], known to be signatures of CMEs. The half without BDES were all cases of fields with solar magnetic polarities matching the surrounding fields, indicating fields locally turned back toward the Sun. An analysis using antisunward propagating Alfven waves [*Kahler*, 1997] on IFRs observed during the heliospheric high-latitude ($\theta > 60°$) passes of the Ulysses spacecraft in 1994 and 1995 also found that all IFRs were due to large-scale turns in the magnetic field [*Balogh et al.*, 1999]. These results support the basic magnetic field topology of the solar source surface model [*Hoeksema*, 1989], which precludes the appearance of small regions of opposite polarity in the source surface dipolar field.

1.3. Structures at SBs

[7] Because the model of the Parker spiral field with superposed turbulence and Alfven waves has been so successful in explaining the IMF structure, little effort has been devoted to understanding either IFRs or the false polarities at SBs. False polarities are defined as solar polarities opposite to those inferred on the basis of the field directions alone [*Kahler et al.*, 1998]. A simple cartoon [*Kahler et al.*, 1996, Figure 3] suggested an ecliptic plane projection of a magnetic flux tube turned back on itself to explain the observed false-polarity fields of the IFRs. A three-dimensional cartoon view of a flux tube coiled backwards around another flux tube of similar polarity to produce a false polarity signature was offered by *Crooker et al.* [1996b].

[8] It is now clear that ICMEs have a major role in SBs, at least during periods of high solar activity. *Crooker et al.* [1998] discussed one SB that was displaced from the HCS by about 45° in solar longitude through a probable reconnection that opened the originally closed field lines of an adjacent ICME. More generally, *Kahler et al.* [1998] found that in 1978–1982 the large-scale sector structure expected from the source surface maps was present, along with a population of small-scale sectors, wedged between the large-scale sectors, with a peak in the time range of 9 hours to 1 day. About half of those small sectors contained periods of BDEs, suggesting that they were ICMEs. In addition, within large magnetic sectors of ≥8 days, the heat-flux BDE signatures of ICMEs were consistent with only rare injections of opposite polarity ICMEs into sectors [*Kahler et al.*, 1999]. The basic picture is that ICMEs are injected into the heliosphere with the polarities of the legs generally matching the ambient field polarities and forming the SBs when observed at Earth. Therefore, contrary to the claim that the HCS cannot penetrate inside the ICMEs [*Smith*, 2001], it appears that the ICMEs reform the HCS.

[9] The heat-flux electron technique was also used to address a view that multiple current sheets at SBs are waves superposed on the HCS by turbulent eddies in the solar wind [*Suess et al.*, 1995]. Because the normals of the field rotations at the current sheets generally lie parallel to those expected for the undisturbed current sheet based on the source surface inclinations [*Behannon et al.*, 1981; *Burton et al.*, 1994], the amplitudes of the proposed waves must be large enough to produce folds in the HCS with sequences of false and true magnetic polarities as defined by the electron heat fluxes [*Crooker et al.*, 1996b]. This wave signature was found neither in a complex SB crossing with 14 field reversals [*Crooker et al.*, 1996b] nor in a survey of the entire 1978–1982 ISEE-3 period [*Kahler et al.*, 1998]. Although some authors [e.g., *Smith*, 2001] think otherwise, the observations have ruled out the wave model [*Crooker*, 1999] for the multiple current sheet encounters at SBs. Note, however, that this does not preclude the existence of shallow waves on the HCS which would produce small (<40°, say) perturbations of the HCS normals.

[10] *Szabo et al.* [1999] looked for true solar magnetic polarity changes in the HCS structure using heat-flux electron analysis of data from the Wind mission from January to July 1995 and from November 1997 to April 1998, periods before and after solar minimum. Of the 60 SB crossings they studied, 48 had a single polarity change and 12 had multiple polarity changes, usually only 3. Fifteen single polarity cases and nearly all the multiple polarity cases were accompanied by at least one BDE event. Five of their HCS crossings were associated with magnetic clouds (MCs). Their results confirm the significant role of ICMEs at SBs but contradict the earlier concept of thick SBs based on the field directional discontinuities [e.g., *Lepping et al.*, 1996].

[11] The advantage of the study periods used in the *Szabo et al.* [1999] work was that the approximate times of the

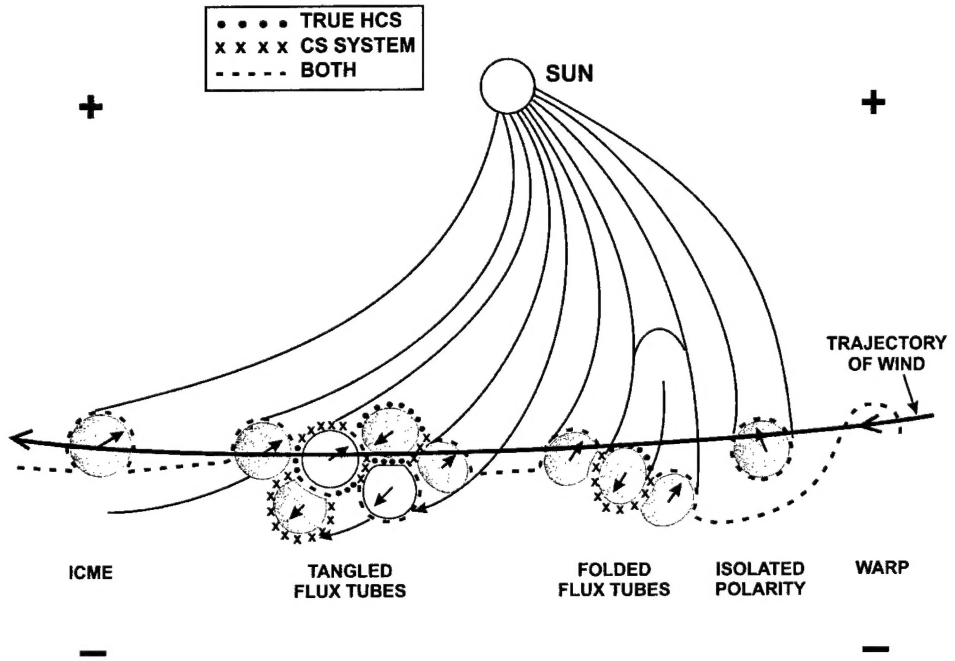

Figure 1. Schematic of the Wind trajectory (heavy line with arrows) along the HCS profile at 1 AU. The successive encounters with candidate features in or near the HCS are a simple warp, an isolated polarity flux tube, a folded flux tube, a cluster of tangled flux tubes, and an ICME leg. The arrows on the flux tube cross sections mark the local field directions. All negative solar-polarity flux tube cross sections are shaded. The shaded flux tubes with the antisunward pointing arrows are due to folded flux tubes. The CS system defined by field reversals is shown by the heavy dashed lines and by the crosses. There is one continuous CS spanning the figure and two separate CSs surrounding the isolated polarity flux tube and one of the tangled flux tubes. The true HCS separates the negative solar polarity fields from the positive polarity fields and is shown by the heavy dashed lines and by the dots. The heavy dashed lines indicate where the CS systems and the true HCS coincide. When the two sheets do not coincide, they are indicated separately by the dots or crosses. The 1996 solar dipole configuration of positive polarity in the north is assumed.

SBs were generally well defined and solar activity was low, allowing a view of the HCS with minimal solar activity. Using data from the same instruments, we will now examine the period of solar minimum when the Wind spacecraft was skimming the HCS. A possible disadvantage of this approach, expressed by *Szabo et al.* [1999], is that the near proximity to the HCS may produce very complex signatures. However, the low inclination of the HCS to the ecliptic also maximizes the interactions between the observer and the HCS and could provide additional insights into HCS structure. Another advantage is that the very minimum of solar activity may reduce some of the IMF complexity observed in the *Szabo et al.* [1999] work.

[12] A schematic view of the trajectory of the Wind spacecraft skimming the HCS is shown in Figure 1. Candidate magnetic features [*Crooker*, 1999] which Wind might encounter as it moves from right to left are a simple warp in the HCS, an isolated opposite (negative) polarity flux tube and surrounding local current sheet (CS), two segments of a folded flux tube, a sequence of tangled flux tubes, and one leg of an ICME or magnetic cloud. The tangled flux tubes were proposed by *Crooker et al.* [1996a] and derive from the associated corrugated current sheet *Villante et al.* [1979] proposed to explain Helios 1 and 2 observations. In this cartoon a CS system separates outward pointing fields from inward pointing fields, regardless of the solar magnetic polarities of the fields. That CS system is shown by the heavy dashed lines and by the crosses. Besides one continuous CS spanning the Wind trajectory, there are two small closed CSs, one surrounding one of the tangled flux tubes and one the isolated polarity flux tube.

2. Data Analysis

2.1. Wind 3-D Plasma and Energetic Particle Experiment Heat-Flux Electron Data

[13] For this study we use data from the Wind 3-D Plasma and Energetic Particle Experiment (3DP), which provides observations of electrons from ~10 eV to ~300 keV and of solar wind speed and density [*Lin et al.*, 1995]. The IMF at Wind was measured with the Magnetic Field Investigation (MFI) [*Lepping et al.*, 1995].

[14] We adopted three basic criteria to select periods for this study. The first is that the Wind orbit be nearly tangential to the HCS to maximize the HCS crossings or interactions. For this criterion we sought periods when the tilts of the HCS to the solar equator, calculated with the classic Stanford 2.5 $R_\odot$ source surface (SS) model (http://quake.Stanford.edu/~wso/coronal.html), were $\leq 21°$. This yielded the period August 1995 to August 1996 and some

Table 1. Period Durations and Polarity Boundary Statistics

Period	C.R. Number	Dates	PAD Intervals[a]	Expected	Transient	Tangent
4	1901–02	1995 01 Oct. to 22 Nov.	135	4	6	4
6	1905–07	1996 03 Feb. to 20 March	140	0	4	6
7	1909–12	1996 20 May to 14 Aug.	256	9	4	12

[a]PAD, pitch angle distribution.

later times. The angular displacements of the HCS relative to the Wind orbit are shown in Plate 1 of *Sanderson et al.* [1998]. The second criterion is that solar activity should be low to minimize encounters with CMEs and shocks. A monthly smoothed international sunspot number ≤ 12 (http://www.sec.noaa.gov/ftpdir/weekly/RecentIndices.txt) limits the period from October 1995 to February 1997.

[15] The last criterion minimizes the IMF connections to the Earth's bow shock, which is a source of energetic electrons that can mimic the heat-flux electrons from the Sun. Bow shock electrons flowing upstream can produce an apparent BDE at Wind when observed in combination with the normal solar wind heat-flux electrons flowing antisunward. We selected periods in which Wind was >90 R_e from Earth, and the Sun-Earth-Wind angle ranged from 345° to 70° measured eastward in the ecliptic plane. We refer to the three selected periods listed in the first column of Table 1 as the periods 4, 6, and 7 of Plate 2 of *Sanderson et al.* [1998]. The second and third columns give the Carrington rotations and dates of the periods.

[16] Wind 3DP summary plots were acquired from the web site (http://plasma2.ssl.berkeley.edu/wind3dp/sumplots/plot_search.html) for all days of the third column of Table 1. Each plot contains one day of solar wind parameters taken from the 3DP and MFI experiments. The pitch angle distributions (PADs) of the 260 eV heat-flux electrons were visually inspected and classified into the following eight categories: 0, a PAD peaked near 0°, signifying a positive field polarity; 180, a PAD peaked near 180°, signifying a negative polarity; diff, a broad (diffuse) distribution with no clear net flow direction and no indication of the field polarity; diff0 or diff180, a broad distribution, but with a net flow direction indicating the field polarity as positive or negative, respectively; bde0 or bde180, a bidirectional electron (BDE) distribution with a dominant flow in the 0° or 180° direction, respectively; or bde, a BDE with no dominant flow direction. Several examples of these PAD intervals are shown in the daily plot of Figure 2. All times throughout the three periods, excepting data gaps (2.3% of the periods), were assigned one of the eight PAD categories. Each reversal in field direction or change in PAD determined the beginning of a new time interval for the analysis. The fourth column of Table 1 gives the numbers of time intervals for each PAD analysis period. The intervals ranged in duration from 0.5 hour, the effective time resolution of the study, to 1 day, with each day counted as at least one interval.

[17] All changes in IMF solar polarity, based only on the 0, 180, diff0, and diff180 PADs, were noted. An example of such a polarity change is shown in Figure 2. The diff, bde, bde0, or bde180 PADs were not considered to be indicators of solar polarity changes. However, in a few cases polarities obviously changed immediately before or after one of the latter PADs, so that the determination of the location of the change was based on other considerations, particularly the IMF direction. The same basic rules were followed by *Kahler et al.* [1998] in classifying magnetic sectors in the ISEE-3 data from 1978 to 1982. An advantage of the 3DP plots is that the times are indicated when the IMF is calculated to be connected to a model bow shock based on the IMF direction and solar wind speed. This calculation provides rough guidance to those times most susceptible to bow-shock electron effects. Apparent BDEs observed at

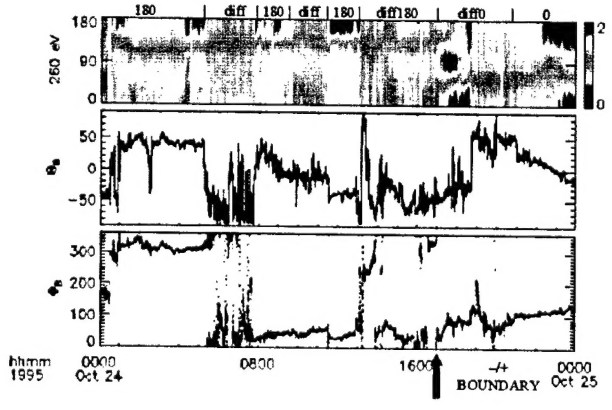

Figure 2. An example of the Wind 3DP heat-flux PADs showing an SB (vertical arrow). Categories for each PAD interval are given above the top panel of electron PADs. The middle and bottom panels are the Θ and Φ angles of the IMF.

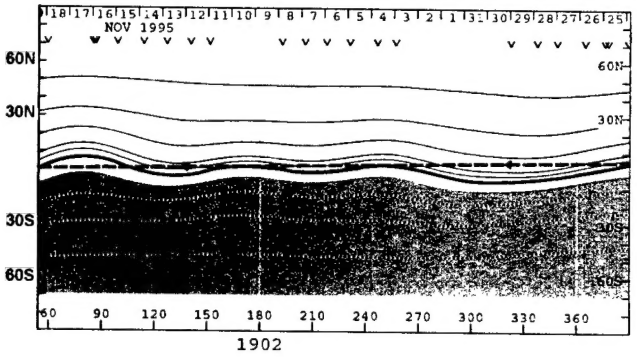

Figure 3. Trajectory of Wind spacecraft (heavy dashed line) projected on the Stanford SS map for Carrington rotation 1902, near the end of period 4. IMF polarity changes at Wind expected on 29 October and 20 November based on the earlier intersections of the Wind trajectory with the HCS were observed on 30 October and 22 November.

those times and considered to be due to the bow shock electrons were noted as a separate category.

2.2. Expected Polarity Boundaries

[18] We used the Stanford SS maps to determine when the solar polarity SBs were expected at Wind. The "Radial Rs = 2.5" model, which assumes a radial photospheric field and yields SS current sheets at R = 2.5 $R_\odot$ of generally low latitudes, was preferred to the classic computation, which assumes that the photospheric field has a meridional component. The superposed Earth trajectory was compared with the HCS (Figure 3) and 5 days added to the HCS crossings to get the expected times of SB crossings at Wind. An observed polarity boundary was found, within 2 days, for each expected SB crossing. The numbers of those crossings for each period are given in the fifth column of Table 1. Note that no SB crossings were expected during period 6 when Wind was south of the calculated HCS.

2.3. Transient and Tangent Events

[19] IMF solar polarity changes presumed due to CMEs were selected in the three analysis periods based on Wind observed magnetic clouds (MC) and interplanetary shocks (http://lepmfi.gsfc.nasa.gov/mfi/) and/or the presence of extensive BDE periods. This resulted in seven pairs (i.e., 14 total, given in the sixth column of Table 1) of polarity changes, with three in October 1995 (MC [e.g., *Larson et al.*, 1997] and BDE), and one each in February (BDE), March (BDE), May (MC), and July (shock) 1996. The seven intervals of these polarity changes ranged from 1 to 48 hours with a median of 21 hours, and in each case a directional flow (0 or 180) or diffuse directional flow (diff0 or diff180) confirmed the change in polarity.

[20] Another eight pairs of possible solar polarity changes were defined by large changes in field direction accompanied by BDEs, but, as discussed in section 2.1, bde PADs do not confirm polarity changes. The intervals of those eight candidates, not counted as transients, ranged from 2 to 9 hours, for a total of only 41 hours, or 0.9% of the three periods. The true BDEs and apparent BDEs possibly resulting from terrestrial bow shock electrons constituted only 2.8% and 2.5%, respectively, of the total durations of the three periods.

[21] A total of 22 remaining solar polarity changes found in the three periods are assumed to result from tangential excursions (given in the last column of Table 1) through the HCS. They ranged in duration from 2 to 53 hours with a median of 7 hours. Only 2 of those 22 changes have a BDE on one side of the boundary. While we assume that the tangential regions are part of the long-lived HCS, we can not rule out the possibility that several of them may have arisen from CMEs or other transient features.

[22] Since the SS maps predict that the HCS lies close to the ecliptic plane during the three periods, it is of interest to examine the ecliptic latitudes of the HCS source regions of the tangent events. In particular, there were four HCS regions, each of duration $\geq$6 days, which lay within about 3° of the ecliptic and would be prime candidates for frequent unexpected HCS traversals if the HCS had a significant wavy structure. One of these skimming regions

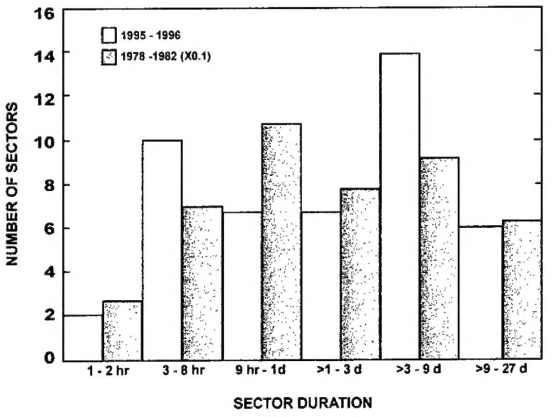

Figure 4. Numbers of polarity sectors as a function of sector duration. Bars on the left are total numbers from the 197 days of the three solar minimum periods of this study, and shaded bars on the right show the comparable totals from the 4-year period of ISEE-3 [*Kahler et al.*, 1998].

from period 4 can be seen in Figure 3, extending from 3–11 November. Two associated tangential excursions of 3 and 53 hours into negative polarities were observed at Wind on 10 November and 15–17 November, respectively. For all three periods, a total of 197 days, 12 of the 22 tangential crossings lay in the 34 skimming-region days. This suggests a clearly increased probability of HCS crossings (35% per day in the skimming regions versus 6% in the remaining 163 days) in accordance with the expected approach of the HCS to the ecliptic, it also means that there were only six excursions, of durations from 1 to 53 hours, across the HCS in those 34 skimming days.

2.4. Distribution of Polarity Sectors

[23] The total number of all solar polarity changes, not counting the 8 pairs of possible changes, is 49 in the three periods. One of the transient polarity changes in period 4, inferred from the change in field direction to occur on 18 October at 1230 UT, lay in a 3DP data gap following a shock [*Larson et al.*, 1997]. Field directions and PADs are available preceding and following the remaining 48 polarity changes of Table 1.

[24] In each period we note the durations of constant polarity, i.e., the magnetic sectors, and show the distribution of those sectors in Figure 4. For context, we compare our distribution with the much larger number of polarity sectors found by *Kahler et al.* [1998] for the ISEE-3 period of 1978–1982. We do not include the polarity sectors bounded by the beginning or ending times of the three intervals, which probably precludes several sectors in the longest time bins. The results for the solar minimum period are not significantly different from those of the 1978–1982 period of high solar activity.

2.5. Statistics at Polarity Changes

[25] To look for significant characteristics that may distinguish fields adjacent to the HCS from fields farther away from the HCS, we examine several field and PAD properties of intervals on each side (preceding and

Table 2. Φ and Θ Rotation Statistics at Polarity Changes

Φ Rotation	Expected	Transient	Tangent	Total[a]
Fast[b]	3	4	13	20(5)
Moderate	4	2	7	13(2)
Slow[c]	6	7	2	15(2)
Total[a]	13(3)	13(3)	22(3)	48(9)

[a]Numbers in parentheses are high-latitude (Θ > 70° over ≥0.5 hour) excursions.
[b]A 90° to 180° rotation in <10 min.
[c]A 90° to 180° rotation in >1 hour.

following) of 48 of the 49 magnetic polarity boundaries of the study periods.

2.5.1. False Polarities

[26] One indicator of the dynamics of field structures at the polarity boundaries is the occurrence of false polarity fields on either side of the polarity boundaries. Seven of those 96 intervals (7%) were false polarities. This is less than the overall false polarity rate for the three periods, which was 65–67 of 531 intervals, or 12–13%, where the higher figure includes two cases of possible polarity changes. The occurrence frequency of false polarities at the polarity boundaries is at most comparable to that of all the intervals of the three periods.

2.5.2. Field Rotation Timescales

[27] The timescale for a large (90°–180°) rotation of the IMF azimuthal angle Φ associated with each polarity change was characterized as slow (>1 hour), moderate (10 min to 1 hour) or fast (<10 min). Those statistics are given in Table 2. The rotations are rather evenly spread over the three timescales, although there is a tendency for the tangent boundaries to be fast rotations and for the expected and transient boundaries to be slower. For at least 11 of the 15 slow changes the exact (within ~3 hours) times of the polarity changes could not be deduced from variations of the IMF directions alone.

[28] The numbers of accompanying IMF high-latitude (hilat) (Θ > 70° over ≥0.5 hour) excursions are given in parentheses in Table 2. Nine of the 48 (19%) polarity changes occurred during high latitude excursions of the field, a figure comparable to the overall figure of 17% hilat associations with the 531 intervals of the three data periods.

2.5.3. Minimum Variance Analysis

[29] Seventeen of the 49 SBs lacked large (≥90°) changes in IMF directions. However, in eight of those 17 cases a fluctuation or rotation of the IMF across the boundary allowed a satisfactory minimum variance analysis of the field to be performed. Of the 32 boundaries with large field reversals we obtained satisfactory fits to all but one, and in one case only a single fit to two closely spaced boundaries, for a total of 30 fits. Figure 5 shows the distributions in inclination (top) and longitude (bottom) of the minimum variance normal vectors. The latitudinal fits are consistent with a random distribution in solid angle, and the longitudinal distribution is peaked between the radial and orthospiral directions.

[30] Note that a small change of field direction across an SB which does not allow for a satisfactory minimum variance analysis must result in either a false polarity on one side of the boundary or a true polarity change across the boundary, depending on the associated heat-flux electron PADs. This is particularly true for near-orthospiral IMF directions. Thus the large fraction of boundaries lacking large changes in IMF directions is not inconsistent with the small fraction of boundaries with false polarities.

2.5.4. Electron PADs

[31] We found the following numbers of PAD categories on the two sides of the 48 polarity changes: 39 (41%) directed (0 or 180), 52 (54%) diffuse (diff, diff0 or diff180), and 5 (5%) in the three bde classes. The upstream and downstream distributions were similar. By comparison, the same directed, diffuse and bde intervals of the three study periods totaled 50%, 39%, and 11%, respectively, of the

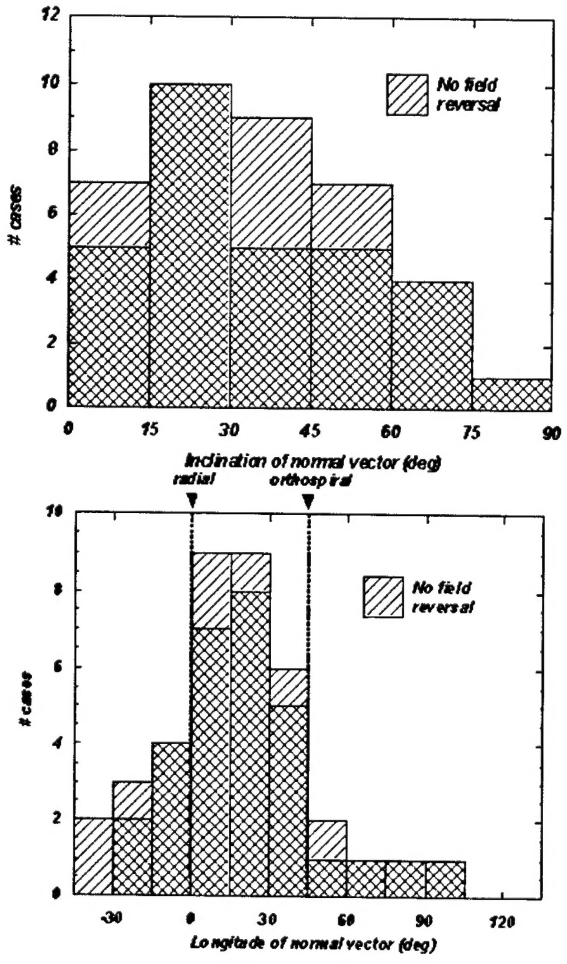

Figure 5. (top) Inclinations to the ecliptic plane of the minimum variance normal vectors of 38 polarity boundaries. Eight cases of boundaries lacking field directional reversals are shown separately. (bottom) Ecliptic longitudinal distribution of the normal vectors.

Table 3. PAD Statistics at Polarity Changes

PAD Type	Expected	Transient	Tangent	Total
Dir/dir	1	2	4	7
Dif/dir	9	6	13	28
Dif/dif(bde)	3	5	5	13

total intervals. There is therefore not a significantly higher association of diffuse PADs with the polarity changes. Table 3 shows the different pairings of upstream and downstream PADs, where we have combined the three bde PADs and the three diffuse PADs into one category, diffuse. The most dominant kind of PAD type is that with a diffuse PAD on one or both sides of the polarity change. Only seven of the 46 polarity changes had directed heat fluxes on each side.

3. Discussion

3.1. Synoptic Polarity Boundary Results

[32] We have used 3DP heat-flux electron PADs to define and examine in detail the solar magnetic polarities of the IMF during the 1995–1996 solar minimum. The selection criteria for the three time periods minimized the probability of encountering solar transient activity and maximized the probability of HCS crossings at small angles to the HCS plane. These crossings should give us an optimal view of the numbers and kinds of magnetic structures composing the HCS.

[33] One remarkable result of the study is that the distribution of sector durations of these periods (Figure 4), when the HCS tilt angles of the Stanford classic SS model were $\leq 21°$, is not much different from that found by *Kahler et al.* [1998] during 1978–1982 when the tilt angles of the same SS model ranged from 41° to 75°. In all the periods of this study the polarity changes expected from the Stanford SS maps were found, along with seven additional sectors (14 boundary crossings), presumed due to ICMEs, and 11 additional sectors (22 boundary crossings) presumed due to additional tangential crossings of the HCS. *Kahler et al.* [1998] explained the smaller (≤ 3 day) sectors of 1978–1982 in terms of CMEs or ejections from helmet arcades at solar polarity boundaries. However, tangential HCS crossings, rather than transient solar activity, may account for most of the smaller 1995–1996 sectors in Figure 4.

[34] The selection of the skimming regions, where the Stanford SS HCS lay within 3° of the ecliptic plane, allowed us to examine more carefully the degree of waviness of the HCS. The increased probability of encountering a wave or corrugation in the skimming region in the form of a tangential excursion (from 6% per day outside the skimming region to 35% per day within the region (section 2.4)) would be expected. However, the limited number of six such excursions during the 34 skimming-region days is consistent with the schematic structure of the HCS suggested by *Crooker et al.* [2001], in which the latitudinal thickness of the HCS was inferred to be ~2°, based on similar heat-flux electron studies for the Wind-Ulysses alignment in 1998.

3.2. Local Polarity Boundary Properties

[35] The properties of the fields and heat-flux electron PADs at the solar polarity boundaries can provide insights into the structures of the HCS. First, we can compare the electron PAD distributions observed at solar polarity boundaries with those of all the intervals and with the results of *Pilipp et al.* [1987], who found heat-flux electron PADs observed on Helios 2 to have antisunward narrow strahls along field lines in sector interiors, but to be isotropic near SBs. We found only a slightly higher tendency for isotropic (our diffuse category) PADs at polarity boundaries (section 2.5.4 and Table 3) than in all the 531 PAD intervals of the study. Thus we do not confirm the basic result of *Pilipp et al.* [1987], although they used directional changes of the IMF as their HCS fiducial while we used solar polarity boundaries of the heat-flux electron PADs, and our observations were limited to within ~20° of the HCS.

[36] The distributions of the normals to the planes of minimum IMF variance at polarity boundaries shown in Figure 5 are very similar to those determined by *Behannon et al.* [1981] for SBs observed by Helios 1. Their distribution of angular inclinations to the ecliptic plane is flat when plotted in terms of equal solid angles, as is our distribution. As *Behannon et al.* [1981] noted, that implies that there is no strongly preferred latitudinal orientation among the planes of the boundaries, and it is similar to that found statistically for IMF tangential discontinuities [*Burlaga et al.*, 1977].

[37] Two measures of disturbed fields are the false polarities and high-latitude excursions. In section 2.5 we found that both these features are also present at polarity boundaries with about the same frequency as those observed away from polarity boundaries.

[38] These statistical results of the PADs, minimum variance normals, false polarities and high-latitude excursions at the polarity boundaries suggest that the magnetic structures at the polarity boundaries are not significantly different from other IMF structures within ~20° of the HCS. The minimum variance normals reflect only the local structures of flux tubes and ropes but not the tilt of the HCS on a global scale, as shown by *Crooker et al.* [2001]. This can be seen schematically in the sections of Figure 1 showing the Wind trajectory through the HCS threading the folded and tangled flux tubes.

[39] Among our 48 solar polarity boundaries were 15 cases for which the timescales of large ($\Phi > 90°$) rotations exceeded 1 hour. In most of those 15 cases, there were no obvious IMF directional changes at the locations of the polarity boundaries. In some cases the reversal of the IMF direction occurred as a gradual rotation over hours and in others the polarity boundary occurred well away from the largest IMF angular rotation. Even in the cases of fast and medium rotational timescales of Table 2, many rotations appeared closer to 90° than to 180°. This result emphasizes that the basic paradigm that the solar polarity boundary coincides with $\omega > 120°$ discontinuities in the IMF direction is simply not valid.

[40] Our results also support a stark difference in complexity between the solar polarity boundary, which defines the HCS, and the large-angle changes of IMF direction around polarity SBs. Treating all large-scale IMF directional changes around SBs as magnetic polarity changes, *Behannon et al.* [1981] and *Lepping et al.* [1996] found >5 and >10 directional discontinuities per SB, respectively. In contrast, *Szabo et al.* [1999], using the same heat-flux electron technique that we use, found that only 12 of 60 SBs were associated with multiple magnetic polarity changes. Similarly, for the 13 expected polarity SBs of our study, only two had either a tangential or transient polarity boundary within one day of those crossings. Thus the interpretation of large-scale IMF directional changes at SBs as solar magnetic polarity changes implies a level

of complexity for the heliospheric magnetic polarity that is inconsistent with the simpler structure inferred from the more direct determination of magnetic polarity from the heat-flux electron analysis. We agree with earlier views of the HCS structure as a tilted, corrugated ribbon [*Villante et al.*, 1979; *Villante and Bruno*, 1982], but we find that the number of solar polarity reversals, and hence the implied degree of corrugation or waviness, is greatly reduced from that of the earlier picture.

3.3. HCS and the Heliospheric Polarity Reversal Sheet

[41] A fundamental difference between our definition of the location of the IMF solar polarity boundary based on heat-flux electron PADs and earlier definitions based on large ($\Phi \geq 120°$) rotations of the IMF directions is that often the two do not coincide. Our observations are consistent with the presence of a single true HCS embedded in a larger, structured CS system [*Crooker*, 2003]. Returning to Figure 1, we show how the true HCS can be separated from the CS system in the cases of the folded and tangled flux tubes. The true HCS separates negative-polarity regions (shaded flux tubes) from positive-polarity regions (unshaded flux tubes), and the CS system separates inward pointing fields (inward arrows) from outward pointing fields. The dashed lines indicate regions where the CS system and the HCS coincide. At the folded flux tube the two sheets separate, with the HCS (dots) lying above the outward pointing negative-polarity flux tube, and the CS system (crosses) under it. At the more complex tangled flux tubes the HCS forms a single continuous sheet of dashed and dotted lines threading the region. The CS system in that region also forms a single continuous sheet of dashed and crossed lines in addition to a separate closed sheet of dashed and crossed lines around the lowermost shaded flux tube.

[42] The HCS at the top of the folded flux tube of Figure 1 shows how a polarity boundary can occur with relatively little change in IMF direction. In that case the adjacent fields are of normal outward pointing positive polarity. A spacecraft traversing the HCS from the adjacent field to the folded flux tube would see no significant change in field direction. Figure 3 of *Crooker* [2003] shows a different perspective of a similar configuration with the HCS lying between parallel field lines. Examples of observed separations of the CS system and the HCS in the IMF where the HCS lies in a relatively unchanging IMF are shown in Figure 3 of *Crooker et al.* [1998] and Figure 2 of *Crooker* [2003]. *Kahler and Lin* [1995] found that for about half the IMF polarity changes of their limited sample the IMF rotation angle $\omega \leq 90°$. In this study we found that about one third (17 of 49) of the polarity boundaries were small-angle ($\leq 90°$) rotations.

[43] Another possibility, shown schematically at the isolated polarity region in Figure 1, is the presence of more than a single HCS if individual flux tubes are sufficiently frayed to lie completely in the opposite polarity hemispheres at 1 AU. Surveys of IFRs in the ISEE-3 [*Kahler et al.*, 1996] and Ulysses [*Balogh et al.*, 1999] observations show that IFRs not associated with ICMEs are false-polarity folds in local fields. The 11 tangential sectors of this study not attributed to expected crossings of the HCS constitute candidates for isolated HCSs. However, the fact that six of the 11 sectors lay within the 3° skimming regions strongly suggests that they are corrugations of a single HCS rather than separate local HCSs. We note that *Smith et al.* [2001] interpret Ulysses sector structure observations at solar maximum in terms of a single boundary between two solar polarity regions that persists to latitudes above 70°.

[44] The HCS is embedded in a distribution of CSs formed by folded flux tubes and IMF directional discontinuities. There must be a single CS girding the entire Sun (the conventional HCS) but also a spectrum of smaller-sized local CSs. The further consideration of helicity in magnetic flux ropes adds the complexity of current volumes in those flux ropes as additional parts of the CS system [*Crooker*, 1999]. Many, if not most, of the large-angle field changes of the CS system around the HCS are not magnetic polarity changes and therefore not part of the HCS itself. *Kahler and Lin* [1995] found that about half of the $\omega > 120°$ discontinuities were not polarity changes and *Szabo et al.* [1999] found that the majority of their large-angle field rotations near the polarity boundary were only local field kinks and not solar polarity changes.

[45] We found in section 2.5 that the magnetic fields at the HCS are not distinguished in any obvious way from the ambient heliospheric fields in terms of false polarities, PADs, minimum variance normals, or high-latitude excursions. We did not separately look for the corresponding properties of large-angle changes characterizing the ambient fields, but we have no reason to expect any difference in these properties between the HCS and those field changes. This further emphasizes the difficulty of trying to identify the HCS by using the field directional changes as a proxy.

[46] The HCS is clarified here as a polarity boundary sheet of the IMF embedded in a larger and more complex CS system [*Crooker*, 2003]. We have argued that the HCS is a simple concept which follows from the extrapolation of the Stanford SS maps to 1 AU and allows us to order the IMF observations far better than could be done with IMF directional measurements in the more complex structure of the CS systems. Combining the in situ IMF directions and polarities should allow us to test models [e.g., *Suess et al.*, 1995] for the solar and interplanetary dynamical origins of the various excursions from Parker spiral fields observed at 1 AU.

[47] **Acknowledgments.** We acknowledge NASA support at Boston University under grant NAG5-10856 and at AFRL under DPR W-19,926.

[48] Shadia Rifai Habbal thanks both referees for their assistance in evaluating this manuscript.

References

Arge, C. N., and V. J. Pizzo, Improvement in the prediction of solar wind conditions using near-real time solar magnetic field updates, *J. Geophys. Res.*, *105*, 10,465, 2000.

Balogh, A., R. J. Forsyth, E. A. Lucek, T. S. Horbury, and E. J. Smith, Heliospheric magnetic field polarity inversions at high heliographic latitudes, *Geophys. Res. Lett.*, *26*, 631, 1999.

Behannon, K. W., F. M. Neubauer, and H. Barnstoff, Fine-scale characteristics of interplanetary sector boundaries, *J. Geophys. Res.*, *86*, 3273, 1981.

Behannon, K. W., L. F. Burlaga, J. T. Hoeksema, and L. W. Klein, Spatial variations and evolution of heliospheric sector structure, *J. Geophys. Res.*, *94*, 1245, 1989.

Burlaga, L. F., J. F. Lemaire, and J. M. Turner, Interplanetary current sheets at 1 AU, *J. Geophys. Res.*, *82*, 3191, 1977.

Burton, M. E., N. U. Crooker, G. L. Siscoe, and E. J. Smith, A test of source-surface model predictions of heliospheric current sheet inclination, *J. Geophys. Res.*, *99*, 1, 1994.

Crooker, N. U., Heliospheric current sheet structure, in *Solar Wind Nine*, edited by S. R. Habbal et al., p. 93, Am. Inst. of Phys., College Park, Md., 1999.

Crooker, N. U., Heliospheric plasma and current sheet structure, in *Solar Wind Ten*, edited by M. Velli et al., in press, 2003.

Crooker, N. U., M. E. Burton, J. L. Phillips, E. J. Smith, and A. Balogh, Heliospheric plasma sheets as small-scale transients, *J. Geophys. Res.*, *101*, 2467, 1996a.

Crooker, N. U., M. E. Burton, G. L. Siscoe, S. W. Kahler, J. T. Gosling, and E. J. Smith, Solar wind streamer belt structure, *J. Geophys. Res.*, *101*, 24,331, 1996b.

Crooker, N. U., et al., Sector boundary transformation by an open magnetic cloud, *J. Geophys. Res.*, *103*, 26,859, 1998.

Crooker, N. U., S. W. Kahler, J. T. Gosling, D. E. Larson, R. P. Lepping, E. J. Smith, and J. De Keyser, Scales of heliospheric current sheet coherence between 1 and 5 AU, *J. Geophys. Res.*, *106*, 15,963, 2001.

Hoeksema, J. T., Extending the Sun's magnetic field through the three-dimensional heliosphere, *Adv. Space Res.*, *9*(4), 141, 1989.

Kahler, S. W., Using charged particles to trace interplanetary magnetic field topology, in *Coronal Mass Ejections*, *Geophys. Monogr. Ser.*, vol. 99, edited by N. Crooker, J. A. Joselyn, and J. Feynman, p. 197, AGU, Washington, D. C., 1997.

Kahler, S., and R. P. Lin, The determination of interplanetary magnetic field polarities around sector boundaries using $E > 2$ keV electrons, *Geophys. Res. Lett.*, *21*, 1575, 1994.

Kahler, S. W., and R. P. Lin, An examination of bidirectional discontinuities and magnetic polarity changes around interplanetary sector boundaries using $E > 2$ keV electrons, *Sol. Phys.*, *161*, 183, 1995.

Kahler, S., N. U. Crooker, and J. T. Gosling, The topology of intrasector reversals of the interplanetary magnetic field, *J. Geophys. Res.*, *101*, 24,373, 1996.

Kahler, S., N. U. Crooker, and J. T. Gosling, Properties of interplanetary sector boundaries based on electron heat-flux flow directions, *J. Geophys. Res.*, *103*, 20,603, 1998.

Kahler, S., N. U. Crooker, and J. T. Gosling, The polarities and locations of interplanetary coronal mass ejections in large interplanetary magnetic sectors, *J. Geophys. Res.*, *104*, 9919, 1999.

Klein, L., and L. F. Burlaga, Interplanetary sector boundaries 1971–1973, *J. Geophys. Res.*, *85*, 2269, 1980.

Larson, D. E., et al., Tracing the topology of the October 18–20, 1995, magnetic cloud with $\sim 0.1-10^2$ keV electrons, *Geophys. Res. Lett.*, *24*, 1911, 1997.

Lepping, R. P., et al., The WIND magnetic field investigation, *Space Sci. Rev.*, *71*, 207, 1995.

Lepping, R. P., A. Szabo, M. Peredo, and J. T. Hoeksema, Large-scale properties and solar connection of the heliospheric current and plasma sheets: WIND observations, *Geophys. Res. Lett.*, *23*, 1199, 1996.

Lin, R. P., et al., Large-dimensional plasma and energetic particle investigation for the WIND spacecraft, *Space Sci. Rev.*, *71*, 125, 1995.

Pilipp, W. G., H. Miggenrieder, K.-H. Mühlhäuser, H. Rosenbauer, R. Schwenn, and F. M. Neubauer, Variations of electron distribution functions in the solar wind, *J. Geophys. Res.*, *92*, 1103, 1987.

Sanderson, T. R., et al., Wind observations of the influence of the Sun's magnetic field on the interplanetary medium at 1 AU, *J. Geophys. Res.*, *103*, 17,235, 1998.

Smith, E. J., The heliospheric current sheet, *J. Geophys. Res.*, *106*, 15,819, 2001.

Smith, E. J., A. Balogh, R. J. Forsyth, and D. J. McComas, Ulysses in the south polar cap at solar maximum: Heliospheric magnetic field, *Geophys. Res. Lett.*, *28*, 4159, 2001.

Suess, S. T., D. J. McComas, S. J. Bame, and B. E. Goldstein, Solar wind eddies and the heliospheric current sheet, *J. Geophys. Res.*, *100*, 12,261, 1995.

Szabo, A., D. E. Larson, and R. P. Lepping, The heliospheric current sheet on small scale, in *Solar Wind Nine*, edited by S. R. Habbal et al., p. 589, Am. Inst. of Phys., College Park, Md., 1999.

Thomas, B. T., and E. J. Smith, The structure and dynamics of the heliospheric current sheet, *J. Geophys. Res.*, *86*, 11,105, 1981.

Villante, U., and R. Bruno, Structure of current sheets in the sector boundaries: Helios 2 observations during early 1976, *J. Geophys. Res.*, *87*, 607, 1982.

Villante, U., R. Bruno, F. Mariani, L. F. Burlaga, and N. F. Ness, The shape and location of the sector boundary surface in the inner solar system, *J. Geophys. Res.*, *84*, 6641, 1979.

N. U. Crooker, Center for Space Physics, Boston University, 725 Commonwealth Avenue, Boston, MA 02215, USA.

S. W. Kahler, Air Force Research Laboratory/VSBXS, 29 Randolph Rd., Hanscom Air Force Base, MA 01731, USA. (stephen.kahler@hanscom.af.mil)

D. E. Larson, Space Sciences Laboratory, University of California, Berkeley, Berkeley, CA 94720, USA.